Alkane activation by silica-supported Group VB metal hydrides. A quantum-chemical study

M. N. Mikhailov and L. M. Kustov*

N. D. Zelinsky Institute of Organic Chemistry, Russian Academy of Sciences, 47 Leninsky prosp., 119991 Moscow, Russian Federation. Fax: +7 (095) 137 2935. E-mail: mik@ioc.ac.ru

A quantum-chemical study of alkane hydrogenolysis and metathesis on silica-supported Group VB metal hydrides (M = V, Nb, Ta) was carried out. Using a model fragment with the β-crystobalite structure permits a correct description of the properties of the grafted organometallic complexes. Alkane hydrogenolysis and metathesis reactions involve (i) π-complexes and carbene complexes of M^{V} and (ii) alkyl derivatives of M^{III} as possible intermediates. The character of the potential energy surfaces of the key alkane transformations points to an important role of triplet states in the catalytic processes involving niobium and vanadium. An alternative low-energy reaction pathway characterized by a change in the spin state was found.

Key words: activation of alkanes, hydrogenolysis of alkanes, metathesis of alkanes, surface metal complexes, Group VB metal hydrides, quantum-chemical calculations, *ab initio* quantum-chemical calculations.

Activation of alkanes remains one of the most important problems in catalytic chemistry. C—C and C—H bond activation in the presence of conventional oxide and bifunctional catalysts proceeds only at temperatures above 300 °C, which requires enormous energy expenditure and enhances side reactions.[1]

Recently, silica-supported transition-metal (Ta, Ti, Zr) hydrides have attracted the attention of researchers.[2] These compounds are synthesized in the reactions of corresponding organometallic compounds with partially dehydroxylated silica followed by reduction of the surface complexes thus formed. Such catalysts can activate the C—C and C—H bonds under mild conditions under which conventional catalysts are inactive.[3,4] In particular, supported tantalum hydride is active in the alkane hydrogenolysis and metathesis reactions (Scheme 1). It is believed[5,6] that the role of the active sites is played by tantalum monohydride and the key stage of transformations is a σ-bond metathesis involving an intramolecular hydrogen exchange when the coordination number of the metal atom remains unchanged. The reaction involves the C—C and C—H bond cleavage. Hydrogenolysis proceeds at a rather high rate and is followed by the formation of lower homologs up to methane; metathesis proceeds at a very low rate and is followed by the formation of the higher and lower homologs.

Scheme 1

$$C_nH_{2n+2} + H_2 \longrightarrow C_{n-1}H_{2(n-1)+2} + CH_4$$

$$2\ C_nH_{2n+2} \longrightarrow C_{n-i}H_{2(n-i)+2} + C_{n+i}H_{2(n+i)+2}$$

$i = 1, \ldots, n-1$

Activation of various alkanes on surface zirconium hydrides has been studied in detail;[7,8] however, information on the structure of active sites and on the mechanisms of reactions involving Group VB metals in unavailable. It is still unclear how the nature of the metal affects the course of these transformations. Obtaining such information is important for target development of new catalysts for alkane activation.

The aim of this work was to carry out a quantum-chemical study of the possibility of alkane activation on silica-supported Group VB metal hydrides (M = V, Nb, Ta) and to determine the structure of possible active sites and the mechanisms of alkane hydrogenolysis and metathesis reactions. This required investigations into the structure of intermediates and transition states (TS) of the key stages in the catalytic cycle of alkane hydrogenolysis and metathesis in the ground and lowest excited electronic states and the establishment of how the nature of the metal affects the behavior of the catalytic system.

Calculation Procedure

Calculations were carried out by the density functional theory (DFT) with the B3LYP exchange-correlation functional as well as by the multiconfiguration self-consistent field (MCSCF) approach. In the latter case, a complete active space (CASSCF)

Published in Russian in *Izvestiya Akademii Nauk. Seriya Khimicheskaya,* No. 2, pp. 296—306, February, 2005.

1066-5285/05/5402-0300

version[9] with inclusion of dynamic electron correlation at the second-order level of perturbation theory (MRMP2)[10] was employed. To reduce the computing time, the SBK pseudopotential[11,12] and the corresponding basis set augmented with polarization functions on all atoms were used in all calculations. The calculations were performed with full geometry optimization, unless otherwise specified. The nature of all stationary points was substantiated by analyzing the Hessians. In addition, for all transition states the reaction pathway was analyzed by the intrinsic reaction coordinate (IRC) method.[13] All calculations were carried out using the GAMESS US program package.[14] The results of calculations were visualized using the MOLDEN [15] and ChemCraft* programs.

Results and Discussion

Structure of active sites. The modified silica surface was modeled by the cluster $(H_4Si_2O_5)(OH)_2$ representing a fragment of SiO_2 β-crystobalite structure[16] in which the broken bonds are saturated with hydroxyl groups whose geometric parameters were fixed in the B3LYP/SBK(d,p) calculations (Fig. 1, *a*). Earlier,[17] it was shown that enlargement of the cluster has almost no effect on the structure of the surface fragment.

Preliminary calculations of the oxidative addition of ethane to tantalum monohydride showed that the catalytic cycles of alkane hydrogenolysis and metathesis on tantalum monohydride are unlikely.[17] Tantalum trihydride was suggested as a possible structure of active sites. The B3LYP/SBK(d,p) optimized structure of the cluster modeling silica-supported tantalum trihydride is shown in Fig. 1, *b*. The Ta—O bond lengths calculated for tantalum trihydride and tantalum monohydride are in good agreement with experimental data (Table 1). IR band frequencies are in much better agreement with the assumption of formation of silica-supported tantalum trihydride characterized by three normal vibrations corresponding to Ta—H stretching vibrations (two symmetrical and one antisymmetrical modes). The calculated stretching vibration frequencies of TaH_3 (Table 2) are in good agreement with experimental data.[18]

Multiconfiguration approach. Analysis of the TS and intermediates in the ground and excited electronic states requires the use of the wave functions that include a number of different electronic configurations. In this connection, possible key stages of the catalytic cycles of alkane hydrogenolysis and metathesis, namely, alkane C—H bond activation; a proton (or alkyl) transfer in the metal carbene to give a complex of the trivalent metal; and dihydrogen addition at the double bond of the metal carbene (Scheme 2) were studied by the CASSCF method, because the CASSCF wave function includes all possible configurations corresponding to all possible combinations of occupation of the active orbitals by the active electrons.

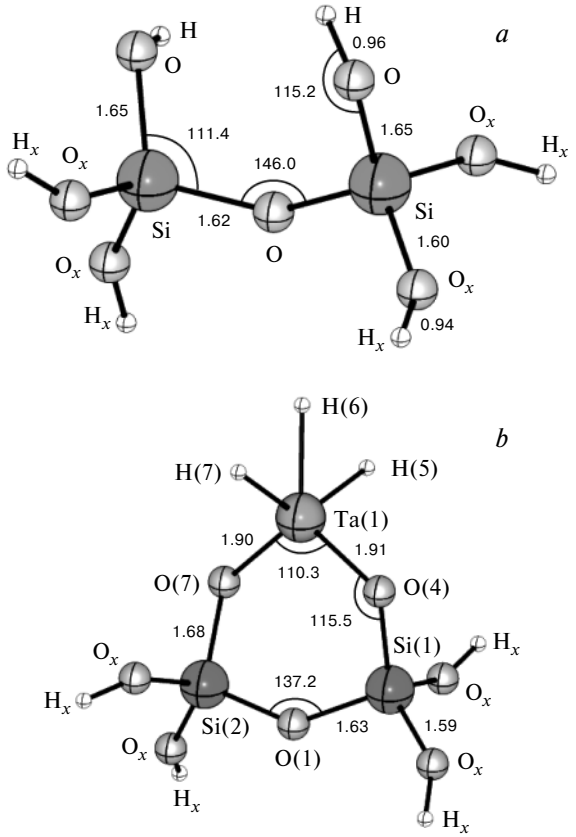

Fig. 1. Structures of cluster $(H_4Si_2O_5)(OH)_2$ (*a*) and a cluster modeling silica-supported tantalum trihydride (*b*) obtained from B3LYP/SBK(d,p) calculations. Here and in Figs 2, 5, 6, 8, 10, and 13 the symbols "O_x" and "H_x" denote atoms which were fixed during geometry optimization procedure. Shown are the bond lengths (in Å) and bond angles (in degrees).

Table 1. Calculated and experimental[18] Ta—O bond lengths (*d*/Å)

Cluster	Calculations		Experiment
	B3LYP	MP2	
$(H_4Si_2O_5)O_2TaH_3$	1.910, 1.901	1.910, 1.907	1.893
$(H_4Si_2O_5)O_2TaH$	1.887, 1.887	1.893, 1.892	1.893

Table 2. Calculated and experimental[18] Ta—H stretching vibration frequencies (ν/cm^{-1})

Vibration	Calculation		Experiment
	B3LYP	MP2	
$\nu_s(TaH_3)$	1913, 1844	1917, 1850	1855, 1815
$\nu_{as}(TaH_3)$	1864	1868	1830
ν(TaH)	1804	1810	—

* Available in the Internet at URL http://www.chemcraftprog.com/.

Scheme 2

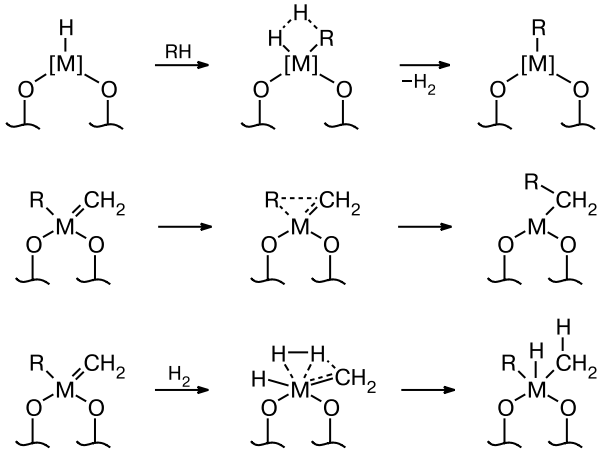

Significance of additional configurations can be evaluated with ease in diagonalization of the first-order density matrix for the CASSCF wave function. If a system is correctly described by the Hartree—Fock method, the eigenvalues of the density matrix will approach a value of two for the bonding orbitals and zero for the antibonding orbitals. The stronger the multideterminant character of the wave function, the higher the populations of the antibonding orbitals. Correspondingly, the bonding orbital populations decrease.[19]

The nature of chemical bonding in transition-metal complexes can be analyzed and interrelations between complex *ab initio* calculations and a simple valence bond approach revealed using the MCSCF/LMO/CI scheme.[20] The approach includes construction of the CASSCF wave function, derivation of MOs localized on atoms to the greatest extent, and construction of the CI wave function with the active space including the localized orbitals. As a result, one obtains (i) contributions of each structure to the wave function of the system and (ii) configurations similar to resonance structures.

Structure of complexes H—[M]$_s$=CH$_2$ ([M]$_s$ = (≡SiO)$_2$M). To describe the structure of metal carbene H—[M]$_s$=CH$_2$ and proton transfer in this system, one must use the active space including six orbitals occupied by six electrons (CAS(6,6) active space). In this case, the singlet-state wave function includes a total of 175 configurations. Correspondingly, it is possible to obtain a total of 175 resonance structures in order to describe such a metal carbene. In spite of the variety of structures, chemical bonding in the system is still quite easy to describe because only the structures with two-center two-electron bonds make the largest contributions. The CASSCF(6,6)-optimized structures of the metal carbenes H—[M]$_s$=CH$_2$ (M = V, Nb, Ta) are shown in Fig. 2. The geometric parameters of the tantalum and niobium complexes are similar, whereas in the vanadium complex the M—O, M—H and M=C bonds are 0.1 Å shorter and the C—M—H bond angle is 5° smaller. The limiting case of applicability of the Hartree—Fock wave function is characterized by the absence of mixing of configurations. This means that the wave function has no biradical character and the natural orbital populations of the bonding σ- and

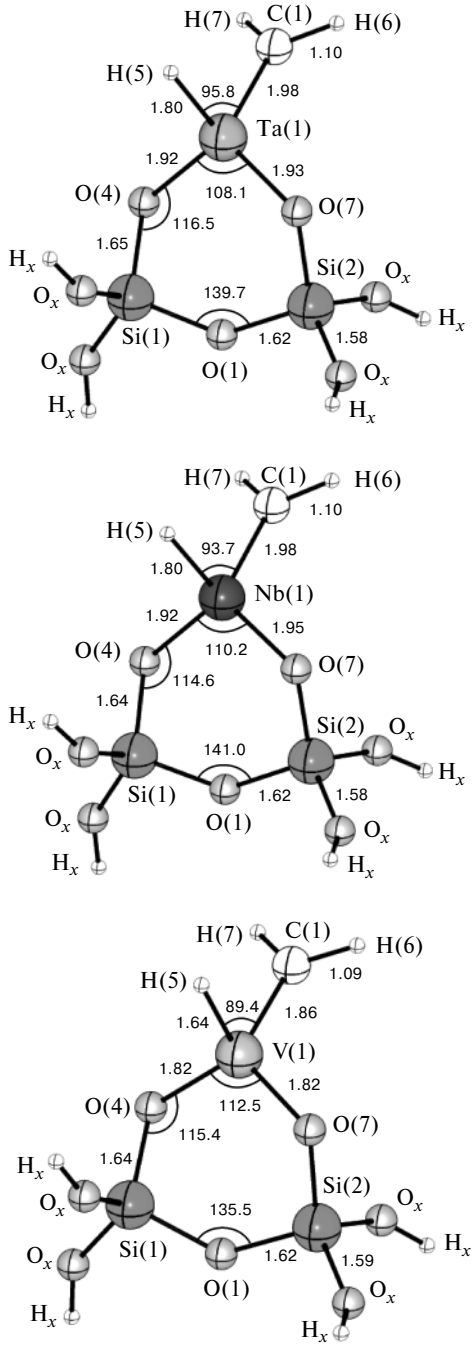

Fig. 2. CASSCF(6,6)-optimized structures of singlet complexes H—[M]$_s$=CH$_2$ (M = V, Nb, Ta). Here and in Figs 3—11 and 13, [M]$_s$ = (≡SiO)$_2$M.

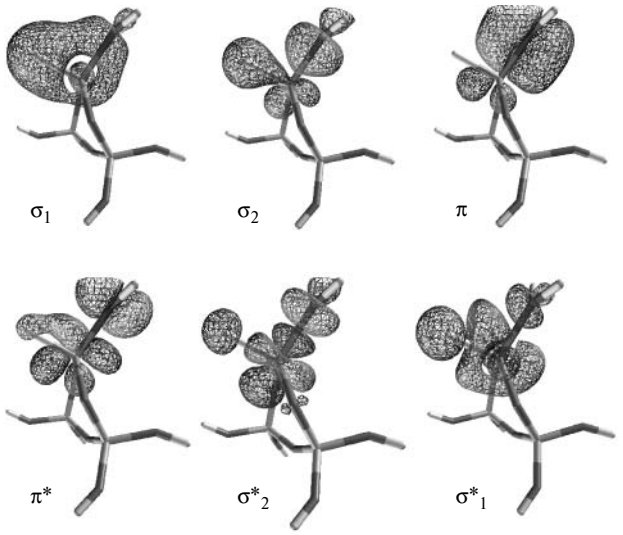

Fig. 3. Natural orbitals of singlet complexes $H—[M]_s=CH_2$ (M = V, Nb, Ta).

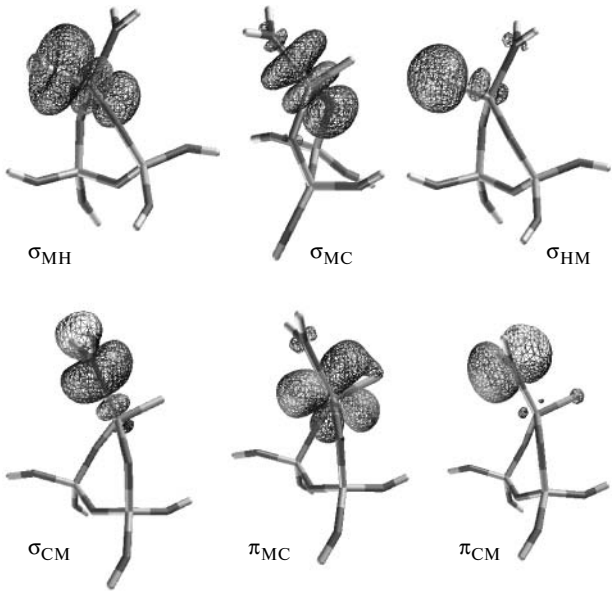

Fig. 4. Localized orbitals of singlet complexes $H—[M]_s=CH_2$.

π-MOs exactly equal two while those of the antibonding σ*- and π*-MOs equal zero. As the biradical character of the wave function increases, the bonding orbital populations decrease while the antibonding orbital populations increase. For a "pure" π-biradical, the bonding π-orbital and the antibonding π*-orbital populations equal unity. The natural orbitals of the complexes $H—[M]_s=CH_2$ are schematically shown in Fig. 3 and their populations are listed in Table 3. The biradical character of the wave function increases in the order Ta < Nb < V and becomes so high for the vanadium complex that the system can no longer be described by the B3LYP method due to divergence of the self-consistency procedure. At the same time the geometric parameters of the niobium and tantalum complexes obtained from CASSCF and B3LYP calculations differ only slightly (by at most 0.04 Å). Since the biradical character implies a high reactivity, the kinetic stability of the systems increases in the order V < Nb < Ta. A correct description of these structures requires the use of the MCSCF wave function, because the antibonding orbital populations become large, especially in the case of vanadium ($n_{\pi^*} = 0.19$).

Table 3. Natural orbital populations of singlet complexes $H—[M]_s=CH_2$

Orbital	M			Orbital	M		
	V	Nb	Ta		V	Nb	Ta
σ_1	1.94	1.96	1.97	π^*	0.19	0.12	0.10
σ_2	1.91	1.95	1.96	σ^*_2	0.09	0.05	0.04
π	1.81	1.88	1.90	σ^*_1	0.06	0.04	0.03

Note. Here and in Tables 4—10, $[M]_s = (\equiv SiO)_2M$.

In order to apply the MCSCF/LMO/CI scheme of analysis, localization of the σ- and π-orbitals according to Ruedenberg[21] was performed separately (Fig. 4). This allowed us to avoid formation of "banana" bonds.

The resonance structures making the major contribution to the wave function of the whole system are listed in Table 4. The contributions of the structures with orbitals occupied by 0, 1, 3, and 4 electrons are negligible. The resonance structures with the carbon atom acting as

Table 4. Contributions (%) of different resonance structures to the wave functions of singlet complexes $H—[M]_s=CH_2$

Resonance structure*	M		
	V	Nb	Ta
H—M⇇C	19.4	15.6	15.3
H—M=C	22.3	23.8	22.3
H→M⇇C	7.8	6.1	5.8
H→M=C	16.3	10.9	9.3
H—M⇄C	4.9	5.2	5.1
H→M⇄C	4.2	2.5	2.2
H←M⇇C	1.8	3.2	3.8
H—M⇆C	5.8	6.1	6.5
H←M=C	1.4	4.3	5.0
H→M⇆C	2.0	2.2	2.4
H—M⇉C	1.5	3.3	3.4
H—M⇄C	1.5	3.2	3.4

* Here and in Table 6 the upper arrow in the resonance structure denotes π-bonding and the lower arrow denotes σ-bonding; a straight line denotes a covalent structure (each of the bonded atoms bears one electron); an arrow denotes an ionic structure (both electrons belong to the atom near the starting point of the arrow), denotes the donor bond.

σ-donor are much more important than the structures in which this atom plays the role of σ-acceptor. Donation from the π_{MC}-orbital of the metal atom to the π_{CM}-orbital of the carbon atom contributes largely to π-bonding. Neutral and nucleophilic structures dominate over electrophilic ones. The greatest contributions to the wave functions of the complexes $H—[M]_s=CH_2$ come from the covalent and σ-donor structures.

The CASSCF(6,6)-optimized structures of triplet metal carbenes $H—[M]_s=CH_2$ (M = Nb, Ta) are shown in Fig. 5. In this case the CASSCF wave function includes a total of 189 configurations. T←S-Excitation causes elongation of the M=C bond by 0.18 Å and rotation of the $=CH_2$ top by 37 (Ta) and 18° (Nb). No minimum corresponding to triplet vanadium complex was located on the potential energy surface (PES). T←S-Excitation of carbene $H—[V]_s=CH_2$ leads to its relaxation immediately into the trivalent vanadium compound $[V]_s—Me$.

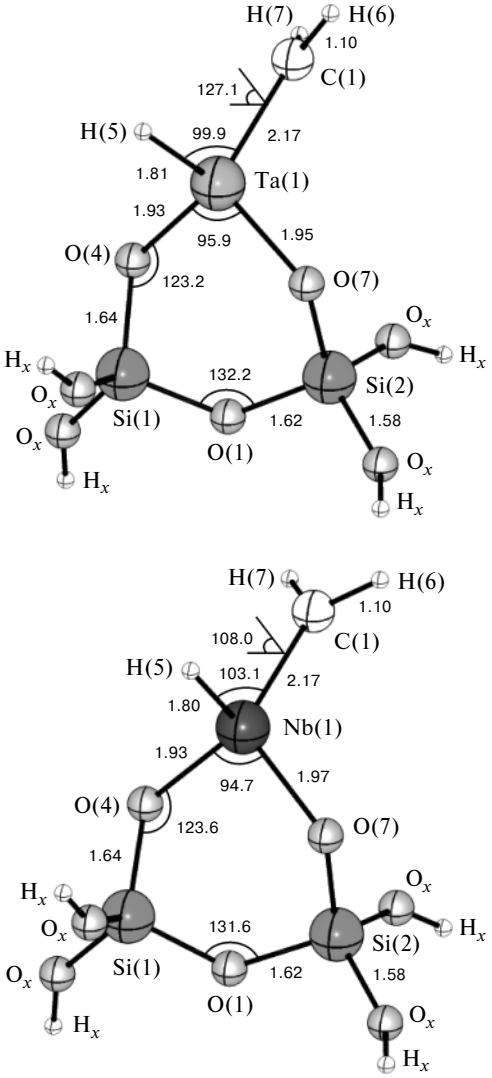

Fig. 5. CASSCF(6,6)-optimized structures of triplet complexes $H—[M]_s=CH_2$ (M = Ta, Nb).

The triplet-state wave function has a much lower biradical character. In the triplet state, there are two equivalent natural orbitals, π_1 and π_2, with unity populations (Table 5) instead of the bonding (π) and antibonding (π*) natural orbitals typical of the singlet state. Analysis of the CI wave function composed of the localized orbitals revealed a 99.8% contribution made by nine resonance structures (Table 6). Similarly to the singlet state, the resonance structures in which the carbon atom acts as σ-donor are much more important than the structures with the carbon atom acting as σ-acceptor. Neutral and nucleophilic structures dominate over electrophilic ones and the largest contributions to the wave function comes from the covalent and σ-donor structures.

The MRMP2 calculated T←S-excitation energies (π—π*-transition) of the $H—[M]_s=CH_2$ complexes are 44 (M = Ta) and 38 kcal mol^{-1} (M = Nb).

Structure of complexes $[M]_s—Me$. The molecular and electronic structures of the singlet complexes $[M]_s—Me$ (M = V, Nb, Ta) are shown in Fig. 6 and in Table 7. The MCSCF and B3LYP calculated geometric parameters of the complexes are similar, except for the M—C bond length. The B3LYP method underestimates this parameter by 0.05 Å compared to the MCSCF scheme.

For all complexes, the major contribution (95%) to the total wave function is made by only three resonance structures with two electrons occupying the n_1 orbital. These are the covalent structure :M—Me (55%), the σ-donor structure :M←Me (30%), and the σ-acceptor

Table 5. Natural orbital populations of triplet complexes $H—[M]_s=CH_2$ obtained from CASSCF(6,6)/SBK(d,p) calculations

Orbital	M		Orbital	M	
	Nb	Ta		Nb	Ta
σ_1	1.98	1.98	π_2	1.00	1.00
σ_2	1.96	1.97	σ^*_2	0.04	0.03
π_1	1.00	1.00	σ^*_1	0.02	0.02

Table 6. Contributions (%) of different resonance structures to the wave functions of triplet complexes $H—[M]_s=CH_2$

Resonance structure	M		Resonance structure	M	
	Nb	Ta		Nb	Ta
H—M⇇C	21.6	20.2	H←M=C	6.4	8.0
H—M=C	34.6	34.6	H—M⇉C	5.5	6.5
H→M⇇C	8.5	7.6	H→M⇉C	2.6	2.8
H→M=C	15.1	13.8	H←M⇉C	0.9	1.4
H←M⇇C	4.3	4.9			

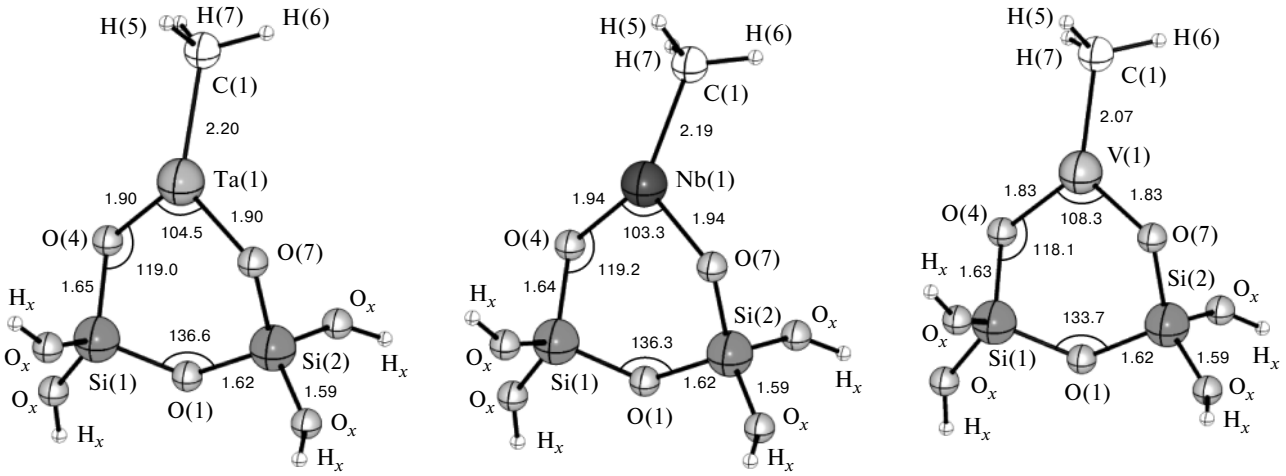

Fig. 6. CASSCF(6,6)-optimized structures of singlet complexes $[M]_s$—Me (M = V, Nb, Ta).

Table 7. Natural orbital populations of singlet complexes $[M]_s$—Me obtained from CASSCF(6,6)/SBK(d,p) calculations

Orbital	M			Orbital	M		
	V	Nb	Ta		V	Nb	Ta
σ_1	1.98	1.98	1.98	n_2	0.03	0.05	0.06
σ_2	1.93	1.97	1.97	σ^*_2	0.07	0.03	0.03
n_1	1.97	1.95	1.94	σ^*_1	0.02	0.02	0.02

Table 8. CASSCF(6,6)/SBK(d,p)-calculated natural orbital populations of triplet complexes $[M]_s$—Me

Orbital	M			Orbital	M		
	V	Nb	Ta		V	Nb	Ta
σ_1	1.98	1.98	1.98	n_2	1.00	1.00	1.00
σ_2	1.97	1.97	1.97	σ^*_2	0.03	0.03	0.03
n_1	1.00	1.00	1.00	σ^*_1	0.02	0.02	0.02

structure :M→Me (10%) (Fig. 7). Neutral and nucleophilic structures dominate over electrophilic ones; their contribution to the total wave function is nearly the same as in the case of the H—$[M]_s$=CH_2 complexes.

A feature of the molecular structure of the $[M]_s$—Me (M = V, Nb, Ta) complexes in the lowest singlet state is nonplanar structure of the OM(C)O fragment, which was not found in the Hartree—Fock calculations. This can be due to a small (1—2%) contribution of the :M—Me resonance structure with two electrons occupying the n_2 orbital to the total wave function of the system. We can suggest that deviation of the methyl fragment from the O—M—O plane by 10 (M = Ta), 16 (M = Nb), and 5° (M = V) is caused by repulsion between two electrons in the n_2 orbital and electrons in the σ_{HC} and σ_{CH} C—H bond orbitals. The molecular and electronic structures of the triplet complexes $[M]_s$—Me are shown in Fig. 8 and in Table 8. As in the singlet-state calculations, the MCSCF and B3LYP calculated geometric parameters of the complexes are similar, except for the M—C bond length (the results obtained differ by 0.06—0.08 Å). T←S-Excitation causes elongation of the M—C bond by 0.05—0.07 Å.

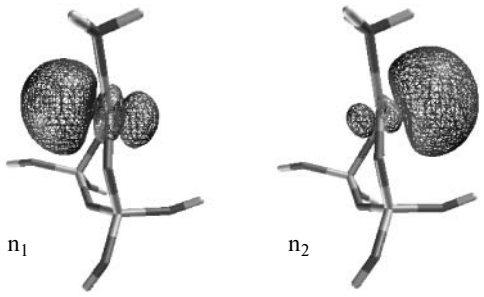

Fig. 7. Localized orbitals n_1 and n_2 of singlet complexes $[M]_s$—Me.

For all complexes, the major contribution (99.5%) to the total wave function make three resonance structures with the n_1 and n_2 orbitals occupied by one electron each. These are the covalent structure M—Me (60%), the σ-donor structure M←Me (25%), and the σ-acceptor structure M→Me (15%) (Fig. 9). As to the vanadium complex, the contribution of the σ-donor structure increases to 30% and that of the σ-acceptor structure decreases to 10%.

The MRMP2 calculated T←S-excitation energy of the $[Ta]_s$—Me complex is 5.5 kcal mol^{-1}. The niobium and vanadium complexes are characterized by the reversed order of electronic energy levels, with the triplet electronic state being the lowest. The MRMP2 calculated singlet-triplet splittings are 9 (M = Nb) and 19.5 kcal mol^{-1} (M = V).

Reactions H—$[M]_s$=CH_2 → $[M]_s$—Me. Proton transfer in the H—$[M]_s$=CH_2 (M = V, Nb, Ta) complexes leads to formation of complexes of trivalent metals, $[M]_s$—Me.

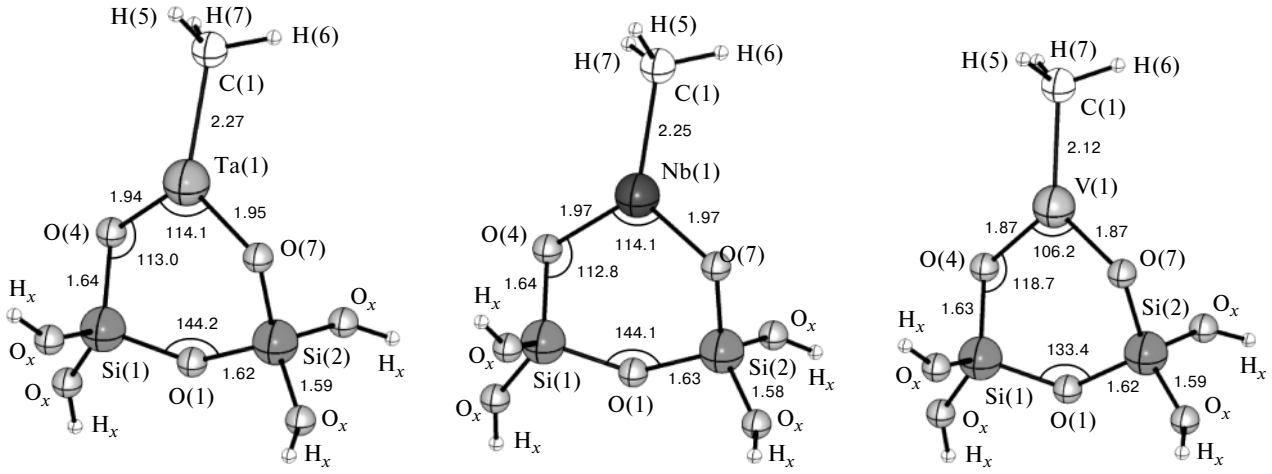

Fig. 8. CASSCF(6,6)-optimized structures of triplet complexes $[M]_s$—Me.

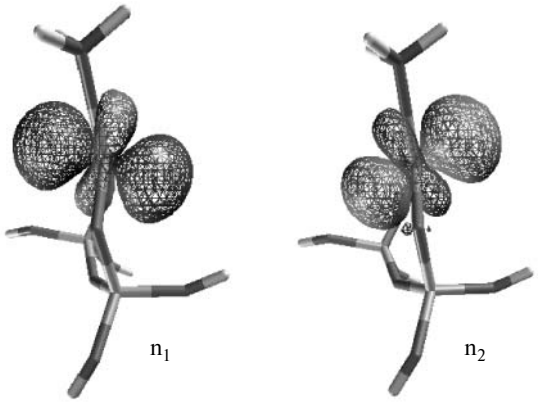

Fig. 9. Localized orbitals n_1 and n_2 of triplet complexes $[M]_s$—Me.

The structures and optimized geometric parameters of the TS of these reactions calculated for the lowest and first excited electronic states are shown in Fig. 10 and listed in Table 9, respectively.

The key role in proton transfer to nucleophilic C atom of metal carbene H—$[M]_s$=CH_2 is played by the interaction of the unoccupied σ*-orbital of the M—H bond with

Table 9. Bond lengths (in Å) in transition states of reactions H—$[M]_s$=CH_2 → $[M]_s$—Me (see Fig. 11)

Bond	M = V	M = Nb				M = Ta			
	CAS(6,6)	CAS(6,6)		B3LYP		CAS(6,6)		B3LYP	
	S	S	T	S	T	S	T	S	T
M—C	1.88	2.03	2.11	1.99	2.08	2.03	2.10	1.99	2.07
M—H	1.70	1.90	1.82	1.85	1.82	1.90	1.85	1.85	1.82
C—H	1.58	1.50	2.13	1.58	2.04	1.49	2.00	1.57	1.90

Note. Symbols "S" and "T" denote the singlet and triplet state, respectively.

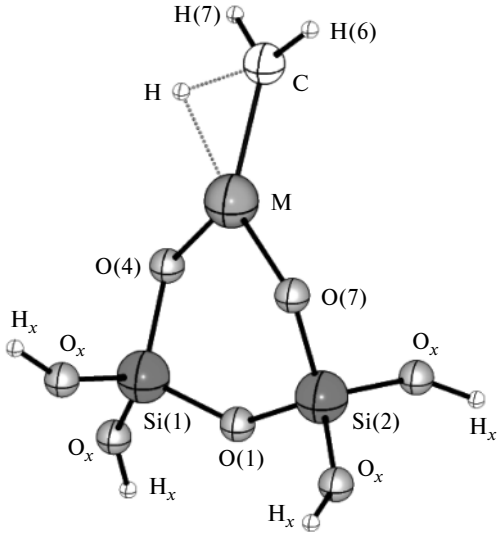

Fig. 10. B3LYP/SBK(d,p)-calculated structures of transition states of reactions H—$[M]_s$=CH_2 → $[M]_s$—Me (M = V, Nb, Ta).

the occupied π-orbital of the M=C bond. This is the so-called electron density back donation from the π-orbital of the M=C bond to the σ*-orbital of the M—H bond.

The singlet and triplet tantalum complexes are characterized by activation barriers of 25 and 12 kcal mol^{-1}, respectively. The reaction involving the singlet complex is endothermic (ΔE = 17 kcal mol^{-1}) while the reaction involving the triplet complex is exothermic (ΔE = −23 kcal mol^{-1}). As a result, the separation between the singlet and triplet PESs reduces to 5 kcal mol^{-1} (Fig. 11, *a*).

A comparison of the potential energy profiles obtained for the singlet (S) and triplet (T) states revealed an important structural feature of the TS. The structure of the triplet TS is similar to the reactant structure while the structure of the singlet TS is more similar to the structure

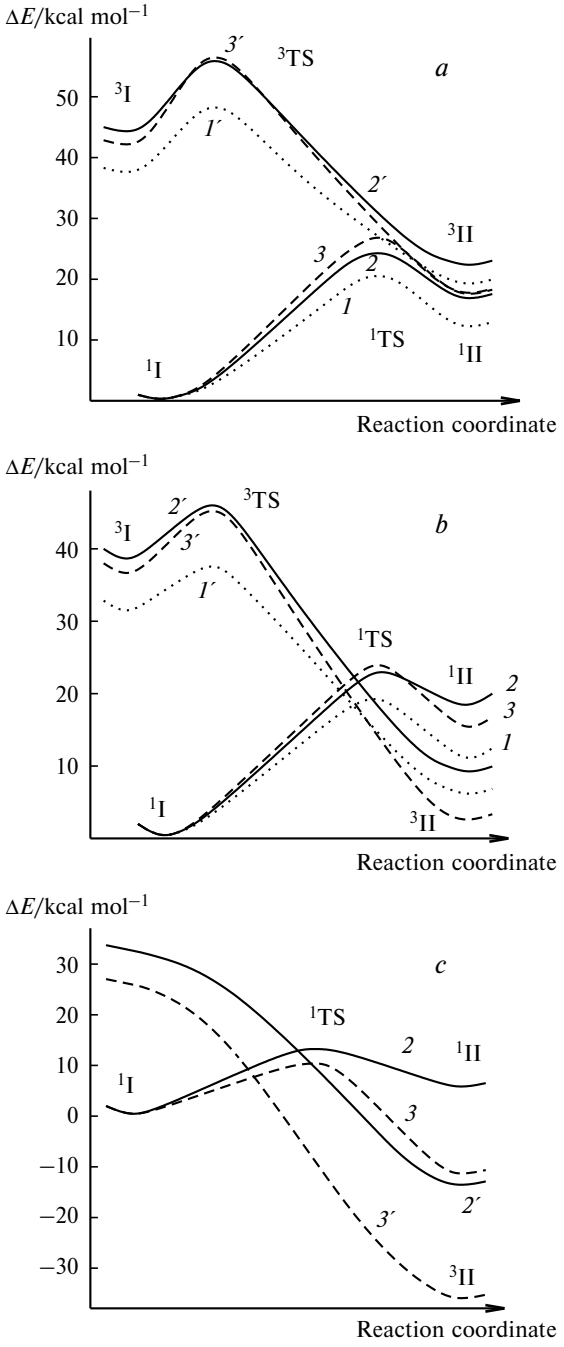

Fig. 11. PES section of the reaction H—$[M]_s$=CH_2 (I) → → $[M]_s$—Me (II) in the ground and lowest excited electronic states; M = Ta (*a*), Nb (*b*), and V (*c*) (TS is transition state). Calculated by the B3LYP (*1*, *1′*), MRMP2 (*2*, *2′*), and CASSCF (*3*, *3′*) methods for the singlet (*1*—*3*) and triplet (*1′*—*3′*) states. Here and in Fig. 12 the left superscripts denote the state multiplicity, namely, singlet ("1") and triplet ("3").

of the product reaction (see Table 9). This difference can play a significant role when considering the reactivity of the niobium and vanadium complexes. For instance, the niobium and tantalum complexes are characterized by similar activation barriers (23 and 9 kcal mol^{-1} for the singlet and triplet states, respectively), the energies of the reaction being 18 kcal mol^{-1} for the singlet PES and −28 kcal mol^{-1} for the triplet PES. The singlet-triplet splitting for H—$[Nb]_s$=CH_2 is 6 kcal mol^{-1} smaller than for H—$[Ta]_s$=CH_2. Because of this, in the former case the singlet and triplet PESs can cross before the barrier is reached (Fig. 11, *b*). The reaction pathway can pass through the PES crossing point rather than the singlet transition state ^{1}TS. This can be accompanied by a multiplicity change and formation of a triplet complex $[Nb]_s$—Me characterized by a singlet-triplet splitting of 9 kcal mol^{-1}. The transition probability between two PESs can roughly be estimated using the Landau—Zener relation.[22] This pathway leads to a decrease in the effective activation energy.

A similar picture was established for vanadium complexes, although no minimum corresponding to the H—$[V]_s$=CH_2 complex was located on the PES of the triplet state. In the singlet state, the activation barrier and the energy of reaction decrease to 12 and 6 kcal mol^{-1}, respectively, and the singlet-triplet splitting for the $[V]_s$—Me complex increases to 20 kcal mol^{-1} (Fig. 11, *c*).

Thus, our calculations show that the stability of the tantalum complexes increases from the triplet complex of Ta^{III} to the singlet complex of Ta^{V}. As to niobium and vanadium, the triplet complex of Nb^{III} occupies an intermediate position and the triplet complex of V^{III} appears to be the most stable form (Fig. 12).

Reactions H—$[M]_s$=CH_2 + H_2 → $[M]_s$—H_2Me (M = V, Nb, Ta). These reactions were described using the active space including eight orbitals occupied by eight electrons (CAS(8,8) active space). The CAS(8,8) active space is the active space of metal carbene H—$[M]_s$=CH_2 augmented with dihydrogen σ_g- and σ^*_u-orbitals. The singlet-state wave function includes a total of 1764 configurations. The structures of TS of these reactions are shown in Fig. 13 and their geometric parameters are listed in Table 10.

The PES sections of the reactions under study are presented in Fig. 14. The activation barriers increase

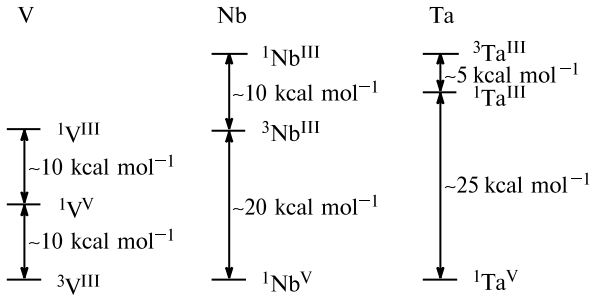

Fig. 12. Relative stability of vanadium, niobium, and tantalum complexes according to the results of MRMP2 calculations.

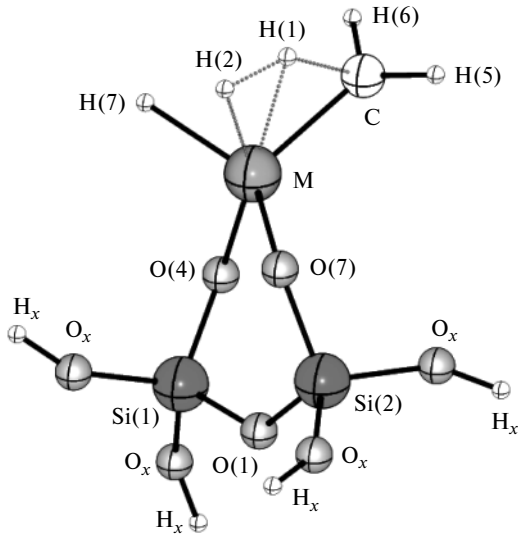

Fig. 13. CASSCF(8,8)-calculated structures of transition states of the reactions $H—[M]_s=CH_2 + H_2 \rightarrow [M]_sH_2Me$ (M = V, Nb, Ta).

slightly from 15 to 19 kcal mol^{-1} and the heats of reactions decrease from 12 to 7 kcal mol^{-1} (exothermic reaction) in order Ta, Nb, V.

Although proton addition at the M=C bond requires a small energy expenditure, activation of C—H bonds in alkanes in the reactions with $H—[M]_s=CH_2$ complexes is a much more difficult process. For instance, the B3LYP/SBK(d,p) calculated activation barrier to alkane addition at the Ta=C bond, resulting in the formation of C—H and Ta—C bonds, is 28 kcal mol^{-1}, being nearly four times higher than the energy needed for proton addition to occur. The interaction between the alkane C—H bond and the M=C bond is governed by the electron density donation from the σ_{CH}-orbital of the C—H bond to the π^*_{MC}-orbital of the M=C bond and by the electron density back donation from the π_{MC}-orbital of the M=C bond to the σ^*_{CH}-orbital of the C—H bond. Owing to steric hindrances the alkane molecule is η^3-coordinated to the metal atom. The M—H—C angle is much larger than it is necessary for efficient orbital overlap to occur and the activation energy for C—C bond formation exceeds 50 kcal mol^{-1}.

Table 10. Bond lengths (in Å) in transition states of reactions $H—[M]_s=CH_2 + H_2 \rightarrow [M]_sH_2Me$

Bond	M = V	M = Nb		M = Ta	
	CAS(8,8)	CAS(8,8)	B3LYP	CAS(8,8)	B3LYP
M—C	1.92	2.04	1.99	2.03	1.99
M—H(1)	1.75	1.91	1.89	1.91	1.89
M—H(2)	1.72	1.88	1.90	1.88	1.90
C—H(1)	1.49	1.55	1.57	1.60	1.62
H(1)—H(2)	1.09	1.10	1.06	1.08	1.04

Note. All calculations were carried out in the SBK(d,p) basis set.

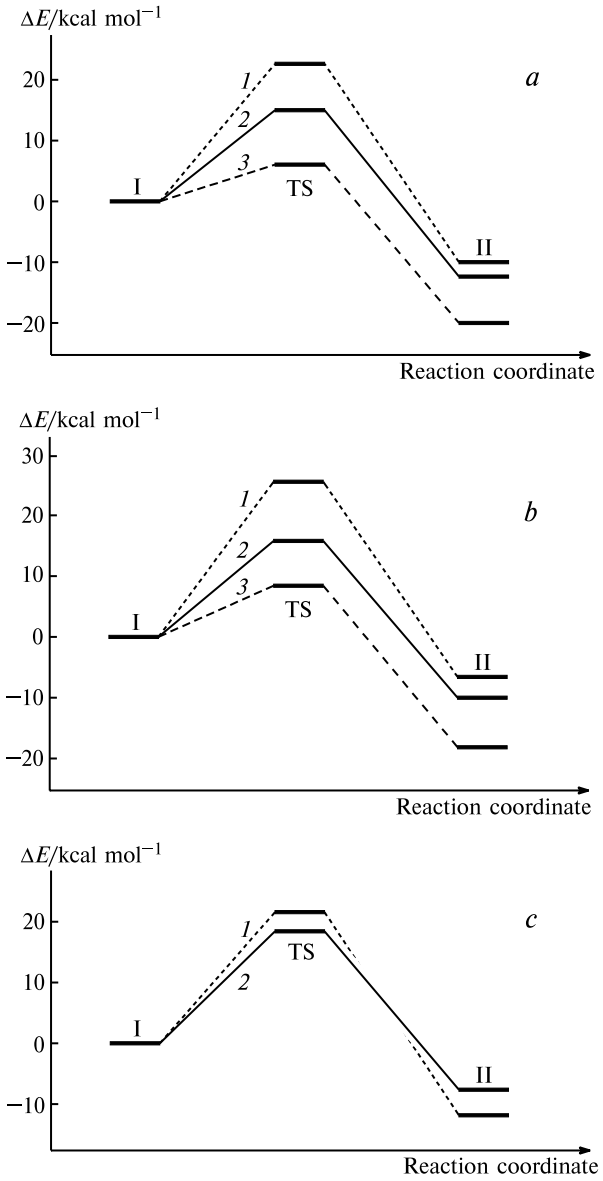

Fig. 14. PES section of the reactions $H—[M]_s=CH_2 + H_2$ (I) $\rightarrow$ $\rightarrow [M]_sH_2Me$ (II) with M = Ta (*a*), Nb (*b*), and V (*c*). Calculated for the ground singlet electronic state by the CASSCF(8,8) (*1*), MRMP2 (*2*), and B3LYP (*3*) methods.

Catalytic cycles of ethane hydrogenolysis. The section of the PES of ethane hydrogenolysis on tantalum trihydride (**1a**)[23] (Scheme 3) is shown in Fig. 15. The process begins with C—H bond metathesis and formation of ethyl dihydride complex **2a**. Elimination of a proton results in metal carbenes **3a**; proton transfer in them leads to formation of a tantalum(III) complex **4a**. Subsequent C—C bond cleavage and Me shift to Ta result in a Schrock carbene **5a**. Further interaction between a proton and the Schrock complex leads to dimethyl hydride complex **6a**.

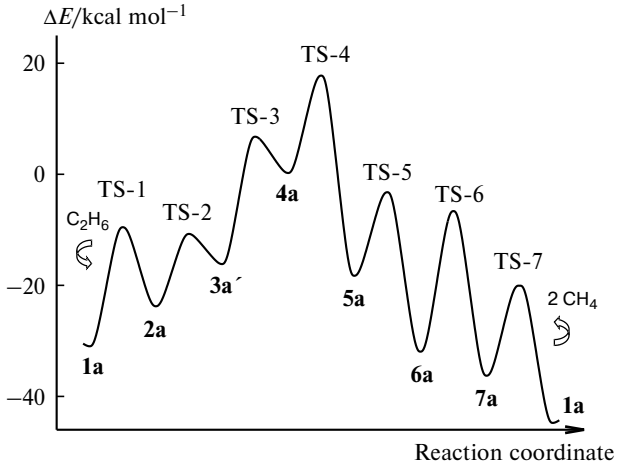

Fig. 15. B3LYP/SBK(d,p)-calculated PES section of ethane hydrogenolysis on tantalum trihydride (**1a**). The structures of the complexes are shown in Scheme 3.

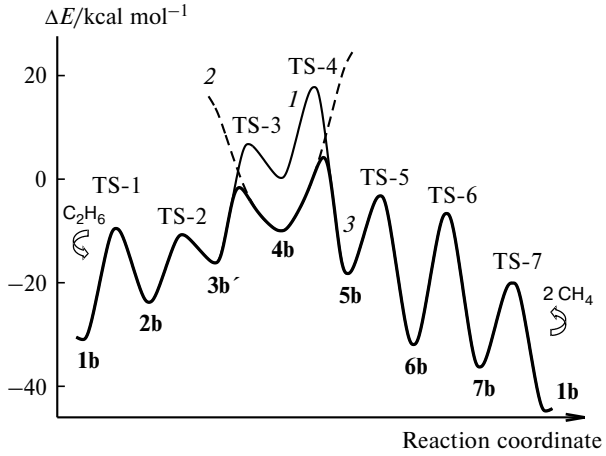

Fig. 16. B3LYP/SBK(d,p)-calculated PES section of ethane hydrogenolysis on niobium trihydride (**1b**): singlet PES (*1*), triplet PES (*2*), and reaction pathway (*3*). The complexes are structurally similar to those shown in Scheme 3 (M = Nb).

The last two stages (**6a** → **7a** and **7a** → **1a**), by analogy with the first stage, represent a σ-bond metathesis and involve regeneration of tantalum trihydride and elimination of methane. Relatively low activation barriers suggest that the catalytic cycle of ethane hydrogenolysis can be realized at relatively low temperatures. Indeed, experiments showed that the reaction does occur at 150 °C.[6]

Nearly identical picture was also established for the catalyst based on niobium trihydride (**1b**). However, the activation energy for the formation of methylcarbene complex decreases due to crossing of the triplet and singlet PESs and emergence of a new low-energy, high-spin reaction pathway. It passes across the singlet PES until the crossing point of the triplet and singlet PESs, goes to the triplet PES, passes through the point corresponding to the triplet state of the ethyl complex **4b**, and again returns to the singlet PES (Fig. 16).

As mentioned above, the most stable vanadium compound is the vanadium(III) complex. In this case the singlet and triplet PESs also cross each other but, in contrast to the reaction involving the niobium complexes, ethane hydrogenolysis begins with C—H bond metathesis in the reaction of ethane with triplet vanadium monohydride resulting in the ethyl complex of vanadium monohydride. Then, the reaction pathway passes through the crossing point of the singlet and triplet PESs corresponding to a

Scheme 3

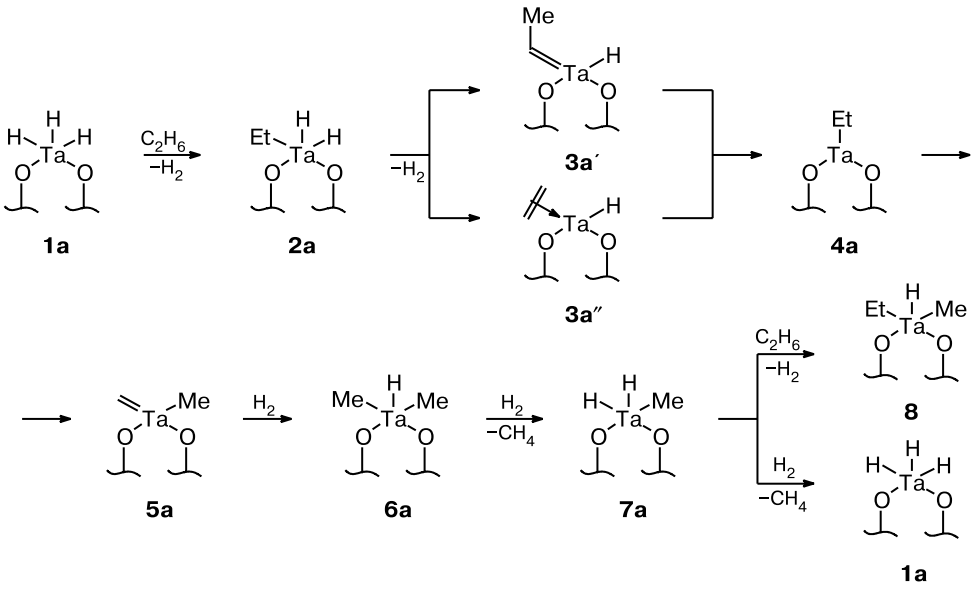

Scheme 4

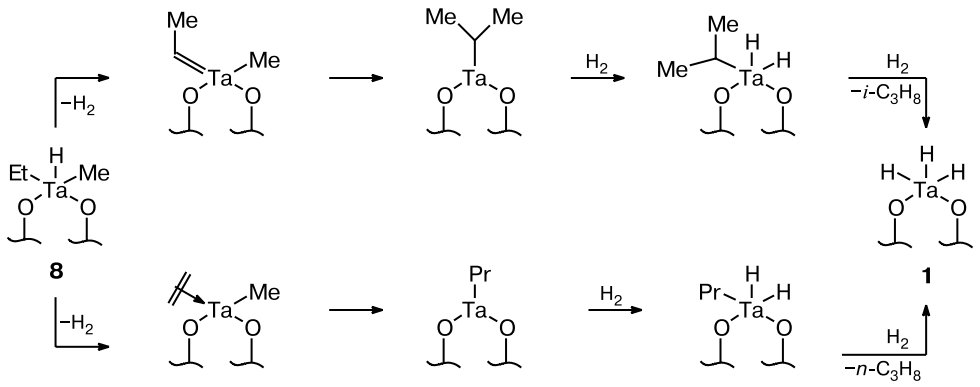

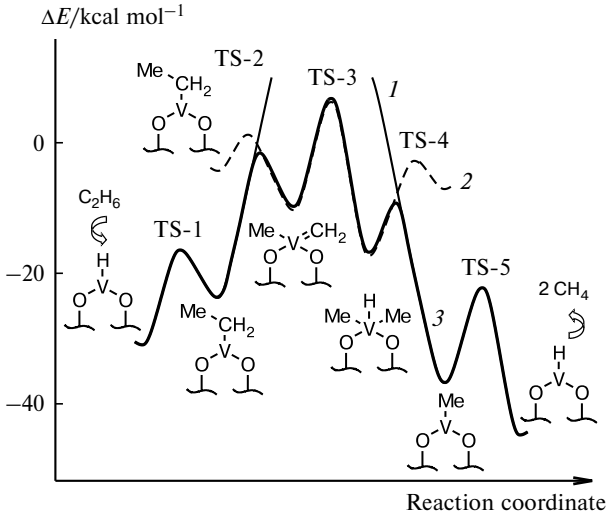

Fig. 17. B3LYP/SBK(d,p)-calculated PES section of ethane hydrogenolysis on vanadium hydride: triplet PES (*1*), singlet PES (*2*), and reaction pathway (*3*).

singlet carbene complex. Further interaction of this complex with hydrogen on the singlet PES results in a dimethyl hydride complex. Then, the reaction pathway passes through the second PES crossing point, the multiplicity changes again, and a methyl complex of trivalent vanadium in the triplet state and methane are formed. The cycle is completed with a process similar to the first stage, which involves regeneration of vanadium(III) monohydride and elimination of yet another methane molecule (Fig. 17).

The catalytic cycle of alkane hydrogenolysis on silica-supported metal hydrides can be used to explain the metathesis of alkanes. A salient feature of the metathesis mechanism is that it permits formation of intermediate alkyl complexes in which the metal atom is bonded to the alkyl fragment through primary or secondary carbon atoms. This provides an explanation for the formation of isomeric alkanes (Scheme 4).

Compared to hydrogenolysis of alkanes, metathesis of these compounds is by and large both thermally and kinetically unfavorable. Such a reaction cannot proceed at rather high rates even at low partial pressures of hydrogen when almost no hydrogenolysis is observed, so it should be considered only as a side reaction accompanying hydrogenolysis of alkanes.

Thus, our calculations showed that possible intermediates of alkane hydrogenolysis and metathesis on silica-supported Group VB metal hydrides are (i) π-complexes and carbene complexes of M^V and (ii) alkyl derivatives of M^{III}. We analyzed peculiarities of the electronic structure of the grafted complexes of Group VB metals and showed that the biradical character of the wave function increases in order Ta < Nb < V. A correct description of the systems based on the vanadium complexes requires the use of the multiconfiguration approach. Based on analysis of the PES structure of the key transformations of alkanes, a possible role of triplet states in the catalytic processes involving the niobium and vanadium complexes was pointed out and an alternative low-energy pathway characterized by the change in the spin state was found.

References

1. N. R. Bursian and S. B. Kogan, *Usp. Khim.*, 1989, **58**, 451 [*Russ. Chem. Rev.*, 1989, **58** (Engl. Transl.)].
2. J.-M. Basset, F. Lefebvre, and C. Santini, *Coord. Chem. Rev.*, 1998, **178—180**, 1703.
3. F. Lefebvre and J.-M. Basset, *J. Mol. Catal. A*, 1999, **146**, 3.
4. F. Lefebvre, J. Thivolle-Cazat, V. Dufaud, P. Niccolai, and J.-M. Basset, *Appl. Catal. A*, 1999, **182**, 1.
5. V. Vidal, A. Theolier, J. Thivolle-Cazat, and J.-M. Basset, *Science*, 1997, **276**, 99.
6. M. Chabanas, V. Vidal, C. Coperet, J. Thivolle-Cazat, and J.-M. Basset, *Angew. Chem., Int. Ed.*, 2000, **39**, 1962.
7. L. Yu. Ustynyuk, Yu. A. Ustynyuk, D. N. Laikov, and V. V. Lunin, *Izv. Akad. Nauk. Ser. Khim.*, 2001, 1959 [*Russ. Chem. Bull., Int. Ed.*, 2001, **50**, 2050].

8. D. V. Besedin, L. Yu. Ustynyuk, Yu. A. Ustynyuk, and V. V. Lunin, *Mendeleev Commun.*, 2002, 173.
9. B. O. Roos, P. R. Taylor, and P. E. M. Siegbahn, *Chem. Phys.*, 1980, **48**, 157.
10. H. Nakano, *J. Chem. Phys.*, 1993, **99**, 7983.
11. W. J. Stevens, M. Krauss, H. Basch, and P. G. Jasien, *Can. J. Chem.*, 1992, **70**, 612.
12. T. R. Cundari and W. J. Stevens, *J. Chem. Phys.*, 1993, **98**, 5555.
13. C. Gonzales and H. B. Schlegel, *J. Chem. Phys.*, 1989, **90**, 2154.
14. M. W. Schmidt, K. K. Baldridge, J. A. Boatz, S. T. Elbert, M. S. Gordon, J. H. Jensen, S. Koseki, N. Matsunaga, K. A. Nguyen, S. J. Su, T. L. Windus, M. Dupuis, and J. A. Montgomery, *J. Comput. Chem.*, 1993, **14**, 1347.
15. G. Schaftenaar and J. H. Noordik, *J. Comput.-Aided Mol. Design*, 2000, **14**, 123.
16. I.-S. Chuang and G. E. Maciel, *J. Phys. Chem. B*, 1997, **101**, 3052.
17. M. N. Mikhailov, A. A. Bagatur´yants, and L. M. Kustov, *Izv. Akad. Nauk. Ser. Khim.*, 2003, 29 [*Russ. Chem. Bull., Int. Ed.*, 2003, **52**, 30].
18. V. Vidal, A. Theolier, J. Thivolle-Cazat, and J.-M. Basset, *J. Am. Chem. Soc.*, 1996, **118**, 4596.
19. M. W. Schmidt and M. S. Gordon, *Ann. Rev. Phys. Chem.*, 1998, **49**, 233.
20. M. S. Gordon and T. R. Cundari, *Coord. Chem. Rev.*, 1996, **147**, 87.
21. C. Edmiston and K. Ruedenberg, *Rev. Mod. Phys.*, 1963, **35**, 457.
22. D. Danovich and S. Shaik, *J. Am. Chem. Soc.*, 1997, **119**, 1173.
23. M. N. Mikhailov, A. A. Bagatur´yants, and L. M. Kustov, *Izv. Akad. Nauk. Ser. Khim.*, 2003, 1827 [*Russ. Chem. Bull., Int. Ed.*, 2003, **52**, 1928].

Received February 6, 2004;
in revised form December 7, 2004